Peer-reviewed version available at *Materials* **2018**, *11*, 398; doi:10.3390/ma11030398

In-situ Reactive Interfacial Compatibilization and Properties of Polylactide/Sisal Fiber Biocomposites via Melt-blending with Epoxy-functionalized Oligomer

Mingyang Hao, Hongwu Wu*, Feng Qiu, Xiwen Wang

The Key Laboratory of Polymer Processing Engineering of Ministry of Education, South China University of Technology, Guangzhou, China

National Engineering Research Center of Novel Equipment for Polymer Processing, South China University of Technology, Guangzhou, China

*Correspondence: mmhwwu@scut.edu.cn (Hongwu Wu)

Abstract: To improve the interfacial bonding of sisal fiber reinforced polylactide biocomposites, polylactide (PLA) and sisal fibers (SF) were melt-blended to fabricate bio-based composites via in situ reactive interfacial compatibilization with the addition of an epoxy-functionalized oligomer (ADR). The FTIR analysis and SEM characterization demonstrated that PLA molecular chain was bonded to the fiber surface and epoxy-functionalized oligomer played a hinge-like role between sisal fibers and PLA matrix, which resulted in improved interfacial adhesion between fibers and PLA matrix. The interfacial reaction and microstructures of composites were further investigated by thermal and rheological analyses, which indicated that the mobility of the PLA molecular chain in composites was restricted because of the introduction of ADR oligomer, which in turn reflected the improved interfacial interaction between SF and PLA matrix. These conclusions were further investigated by the calculated activation energies of glass transition relaxation (ΔE_a) of composites via dynamic mechanical analysis. The mechanical properties of PLA/SF composites were simultaneously reinforced and toughened via addition of ADR oligomer. The interfacial interaction and structure-properties relationship of composites are key points of this study.

Keywords: polymer-matrix composites; natural fiber reinforcement; interface/interphase; microstructural analysis; crystallization behavior; rheological behavior.

Peer-reviewed version available at Materials 2018, 11, 398; doi:10.3390/ma11030398

1. Introduction

Due to increasing concerns about environment and sustainability issues, natural fibers have attracted extensive attention for its ecological and renewable sustainable nature. The development of natural fiber-reinforced polymer composites has attracted wide attention both in academia and industry, for their low cost, light weight, ability to recycle, good structural properties and so on [1-4].

The mechanical properties of fiber-reinforced polymer composites not only influenced by the intrinsic properties of fibers and polymer matrix, but also are affected by the interfacial properties of composites [5]. The stress is transferred from polymer matrix to fibers via interface of composite under load-bearing. Therefore, a fundamental study of the fiber-matrix interface is critical to the development of fiber-reinforced polymer composites. Numerous studies have proved that a good interfacial adhesion is of great importance for obtaining good mechanical properties of composites materials [6]. Good interfacial compatibility between fibers and polymer matrix will result in efficient stress transfer from matrix to the fiber, so improve the mechanical performance of composites. For natural fiber-reinforced polymer composites, the interfacial compatibility between natural fibers and matrix is generally poor due to the hydrophilic nature of natural fiber and the hydrophobic nature of polymer matrix. In natural fibre-reinforced polymer composites, the two phases are mechanical and/or chemically combined, and the fibre-matrix interface can be considered as a diffusion or reaction zone. Poor chemical and physical interfacial interaction between natural fiber and polymer matrix are considered as the most important mechanisms of bond failure.

To improve the interfacial interaction of natural fiber-reinforced polymer composites, many surface modification methods were applied to natural fibers to improve the compatibility between fibers and matrix [7]. It had been proved that chemical treatments of natural fiber surface were an effective way to improve the interfacial compatibility and adhesion of natural fibre-reinforced polymer composites [8]. Several types of chemical treatment methods were developed for surface modification of natural fiber, including silane treatment [9,10], acetylation treatment [11], benzoylation treatment [12], acrylation and acrylonitrile grafting [13,14], dopamine treatment [15], N-methylol acrylamide grafting [4] and so on. Alkali treatment with sodium hydroxide is one of the most widely used chemical treatment methods for natural fibers [16,17]. It can remove the lignin, natural fats, waxes and impurities for natural fiber surface. Therefore the surface roughness of natural fibers is improved and more reactive functional groups on fiber surface are revealed. Alkali treatment with sodium hydroxide has been widely used before other chemical treatment is performed in natural fibers surface modification, because it can expose more hydroxyl groups and other reactive functional groups on natural fibers surface, thus promote the interfacial interaction [18]. These chemical treatment methods could improve

Peer-reviewed version available at Materials 2018, 11, 398; doi:10.3390/ma11030398

interfacial adhesion of natural fibres and polymer matrix, but sometimes weaken the fibre strength itself at the same time. Furthermore, these methods generally take a long time to soak natural fibres in corresponding solution, thus they are inefficiency. Meanwhile, the organic solvents used in these methods are usually not friendly to environment. Reaction processing can improve the interfacial compatibility of composites via in-situ reaction during melt-blending processing, thus it is a promising method to prepare natural fibre-reinforced polymer composites without the disadvantages of chemical treatment methods.

Joncryl ADR®-4368 is a kind of commercial grade multi-epoxy-functionalized styrene-acrylic oligomer (ADR) [19-21]. We consider that ADR has a potential to be an efficient reactive compatibilizer in natural fiber reinforced polymer composites. In this study, polylactide and sisal fibers were used to fabricate bio-based natural fiber reinforced polymer composites. To improve the interfacial adhesion of PLA/sisal fibers composites, polylactide resin and sisal fibers were melt-blended via in-situ reactive interfacial compatibilization with addition of ADR oligomer. The in-situ reaction processing method has the possibility of bonding PLA molecule chain onto the fiber surface via interfacial reaction of the functional groups on natural fibers surface and the end group of PLA. The phase morphology, thermal behaviors, rheological behaviors, dynamic mechanical analysis and tensile properties of PLA/sisal fiber composites were investigated. The interfacial interaction and structure-properties relationship of composites are key points of this study.

2. Experimental section

2.1. Materials

The PLA (trade name 4032D), a semi-crystalline extrusion grade with 1.2-1.6 % D-isomer lactide and density of 1.25 g/cm^3, from Nature Works LLC (Minnesota, USA) was used. It was dried in an air dry oven at 80 ℃ for 8h before use. The chopped sisal fibers (6 mm) were purchased from Dongfang Sisal Co. (Guangdong, China) and the properties of the fiber provided by supplier were shown in Table 1. Joncryl ADR®-4368 was provided by Shanghai Kingpont Chemical Company, China P. R.

Table 1. Properties of sisal fibers.

Fiber diameter (μm)	Fiber density (g/cm^3)	Cellulose content (%)	Hemicellulose content (%)	Lignin content (%)
25-200	1.45	67-78	10-14	8-11

2.2. Preparation of the composites

Sisal fibers were soaked in sodium hydroxide solution (5 wt %) for 1h to remove lignin, pectin and waxy

Preprints (www.preprints.org) | NOT PEER-REVIEWED | Posted: 6 February 2018 doi:10.20944/preprints201802.0049.v1

Peer-reviewed version available at Materials 2018, 11, 398; doi:10.3390/ma11030398

substances on sisal fibers surface, then vacuum dried at 80 ℃ for 8h. Melt blending of PLA, sisal fibers (SF) and ADR was performed using an internal mixer (Poton 100, China) at 200 ℃ for 5 min with a roller speed of 80 rpm. A series of PLA/SF and PLA/SF/ADR composites with different ADR addition and different SF content were prepared. Then, the obtained mixtures were compression-molded at 200 ℃ for 3 minutes under 10 MPa into standard specimens for rheological dynamic frequency sweep tests and mechanical tests. At the same time, to characterize the internal reaction of the composites melt, rheological dynamic time sweep tests were performed in this study. Thus the PLA/SF/ADR composites samples were prepared using internal-mixer at a relatively low temperature (180 ℃) for 2 min without any further melt processing. The dynamic time sweep tests were executed at a melt mixing temperature of 200 ℃.

2.3. Measurements of tensile properties

Notched Izod impact tests were performed following the ISO 180, using a 5.5 J pendulum at room temperature. The tensile tests were carried out on a universal tensile testing machine (Instron 5566, USA) according to ISO 527-2 with a crosshead speed of 2 mm/min. At least five specimens for each composite were tested. The average values were calculated and the standard errors were obtained as well.

2.4. Morphological characterization

The specimens after the tensile tests and Izod impact tests were used for morphological characterization. The tensile and impact fracture surfaces morphology of the composites was recorded by scanning electron microscope (SEM, FEI Quatan 250, USA). Fracture surfaces were sputtered with gold before SEM observation to provide enhanced conductivity.

2.5. The FTIR measurement

In order to estimate the interfacial bonding between PLA and sisal fibers via reaction with ADR oligomer during the melt-blending processing, the sisal fibers were obtained from composites by Soxhlet extraction[] using dichloromethane as solvent and dried at 80 ℃ for 8 h in a vacuum oven, and then grinded into powder for FTIR analysis. The FTIR spectroscope (Nexus 670, Thermo Nicolet Co. Ltd, USA, KBr powder) was used to characterize the extracted fibers over a range of 4000-400 cm^{-1}. For comparison, FTIR characterization of PLA resin was also carried out.

2.6. Thermal analysis

The thermal behavior of composites was studied using a differential scanning calorimeter (DSC-204C, NETZCH, Germany). For isothermal melt crystallization, the samples were heated from 30 ℃ to 190 ℃ and held for 5 min at 190 ℃ to eliminate the thermal history, and then cooled down to 110 ℃ at a rate of 50 ℃/min and held for a period of time until the isothermal crystallization was complete. The isothermal crystallization

Peer-reviewed version available at Materials 2018, 11, 398; doi:10.3390/ma11030398

behaviors at different crystallization temperature were also performed. For non-isothermal melt crystallization, the samples were first heated from room temperature to 190 ℃ and held for 5 min to eliminate the thermal history, and then cooled back to 30 ℃ at a rate of 10 ℃/min. After 2 min in 30 ℃, the second heating scan from 30 ℃ to 190 ℃ at 10 ℃/min was performed. The cooling-crystallization of PLA/SF/ADR composites at 5 ℃/min was also carried out. In the whole process, all samples were kept under nitrogen flow of 25 ml/min.

2.7. Rheological characterization

Viscoelastic behavior of composites was measured by a dynamic oscillatory rheometer (Anton paar, MCR 302, Austria), equipped with a plate diameter of 25 mm and a gap of 1 mm parallel plate geometry. The following tests were performed: a) dynamic small amplitude oscillatory frequency sweep tests from 0.0628 rad/s to 628 rad/s at 180 ℃ with a strain amplitude of 1%; and b) dynamic time sweep test using 1% strain amplitude and an angular frequency of 10 rad/s at 200 ℃.

2.8. Dynamic mechanical analysis (DMA) testing

The DMA measurements (DMA-242 E, NETZSCH, Germany) were carried out at 0.1, 0.5, 1.0, 5 and 10 HZ respectively under a heating rate of 2 ℃/min, using three point bending 40 mm measurement method. The temperature range was from 30 ℃ to 110 ℃.

3. Results and discussion

3.1. Morphology analysis

The impact fracture surfaces of PLA/SF and PLA/SF/ADR composites with constant 20 wt% SF content and different ADR addition are shown in Figure 1. It can be seen from Figure 1(a), for PLA/SF composites many fibers were directly pulled out from PLA matrix, and many holes were formed in the fracture surfaces, reflecting poor interfacial adhesion between PLA matrix and sisal fibers. However, the addition of ADR into composites during melt-blending processing could effectively counteract this phenomenon, as shown in Figure 1(b-f) for which ADR content varied from 0.2 wt% to 1.0 wt%. For PLA/SF/ADR composites, the fibers were tightly connected with matrix and underlay the matrix, and it was observed that more fibers were broken up or torn off in composites with ADR addition compared with that of PLA/SF composites. These phenomena demonstrated the improved interfacial adhesion of PLA/SF/ADR composites via addition of ADR compared with that of PLA/SF composites. In order to further confirm this result, the impact fracture surfaces of PLA/SF composites and PLA/SF/ADR composites with different SF content are presented in Figure 2. For PLA/SF composites, the similar phenomena were observed. Many fibers were directly pulled out from PLA matrix and many holes were formed in the fracture surfaces, reflecting poor interfacial adhesion (Figure 2a-d). It was also observed that the more SF was added, the more fracture defect occurred. The presence of ADR improved the interfacial adhesion

Preprints (www.preprints.org) | NOT PEER-REVIEWED | Posted: 6 February 2018 doi:10.20944/preprints201802.0049.v1

Peer-reviewed version available at Materials 2018, 11, 398; doi:10.3390/ma11030398

between SF and PLA matrix (Figure 2e-h). Furthermore, the tensile fracture surfaces of PLA/SF composites and PLA/SF/ADR composites with different SF content are shown in Figure 3. It can be seen from Figure 3(a)-(d) that the sisal fibers were directly pulled out from PLA matrix in PLA/SF composites, which impair the reinforce effect of SF during tensile tests. However, for PLA/SF/ADR composites, the improved interfacial adhesion between SF and PLA matrix cause that many fibers were broken up or torn off in the tensile fracture surface, which indicated that the fibers bore the load in the tensile tests.

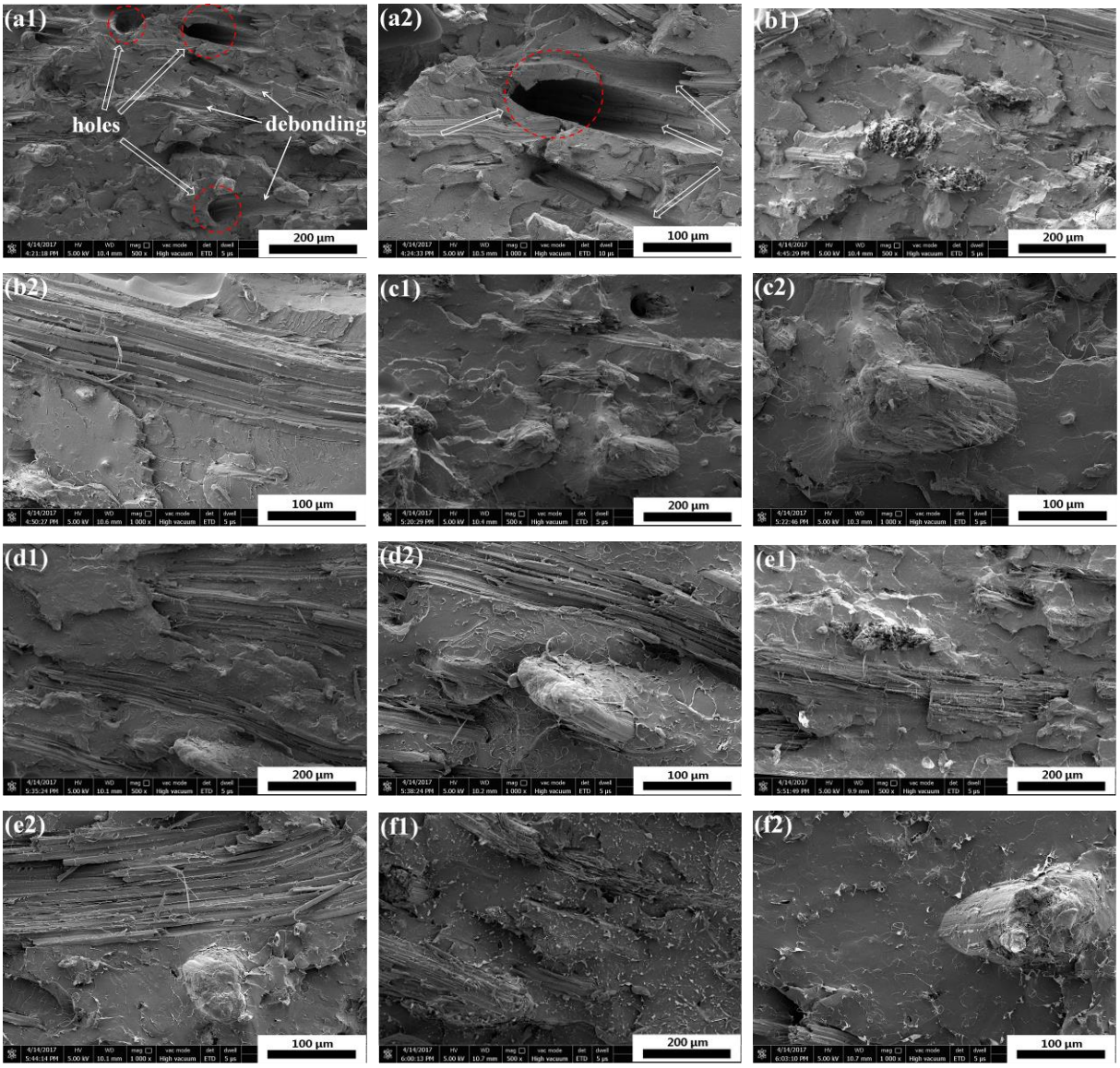

Figure 1. The impact fracture surfaces of PLA/SF (80/20) (a1, a2) and PLA/SF/ADR composites with different ADR content: (80/20/0.2) (b1, b2); (80/20/0.4) (c1, c2); (80/20/0.6) (d1, d2); (80/20/0.8) (e1, e2); (80/20/1.0) (f1, f2).

Preprints (www.preprints.org) | NOT PEER-REVIEWED | Posted: 6 February 2018 doi:10.20944/preprints201802.0049.v1

Peer-reviewed version available at Materials 2018, 11, 398; doi:10.3390/ma11030398

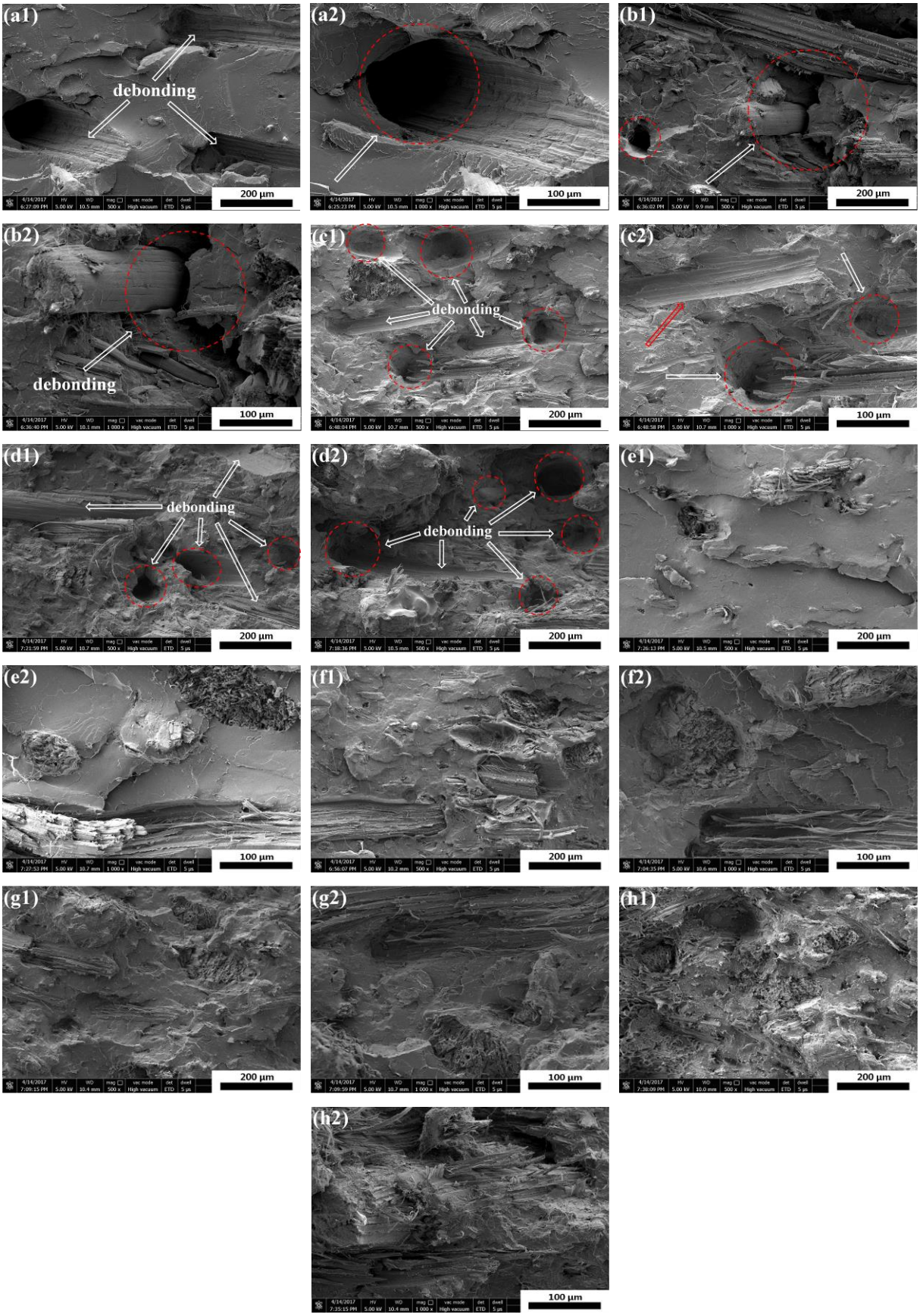

Figure 2. The impact fracture surfaces of PLA/SF composites (90/10) (a1, a2); (80/20) (b1, b2); (70/30) (c1, c2); (60/40) (d1, d2) and PLA/SF/ADR composites (90/10/0.6) (e1, e2); (80/20/0.6) (f1, f2); (70/30/0.6) (g1, g2); (60/40/0.6) (h1, h2) with different SF content.

Preprints (www.preprints.org) | NOT PEER-REVIEWED | Posted: 6 February 2018 doi:10.20944/preprints201802.0049.v1

Peer-reviewed version available at Materials 2018, 11, 398; doi:10.3390/ma11030398

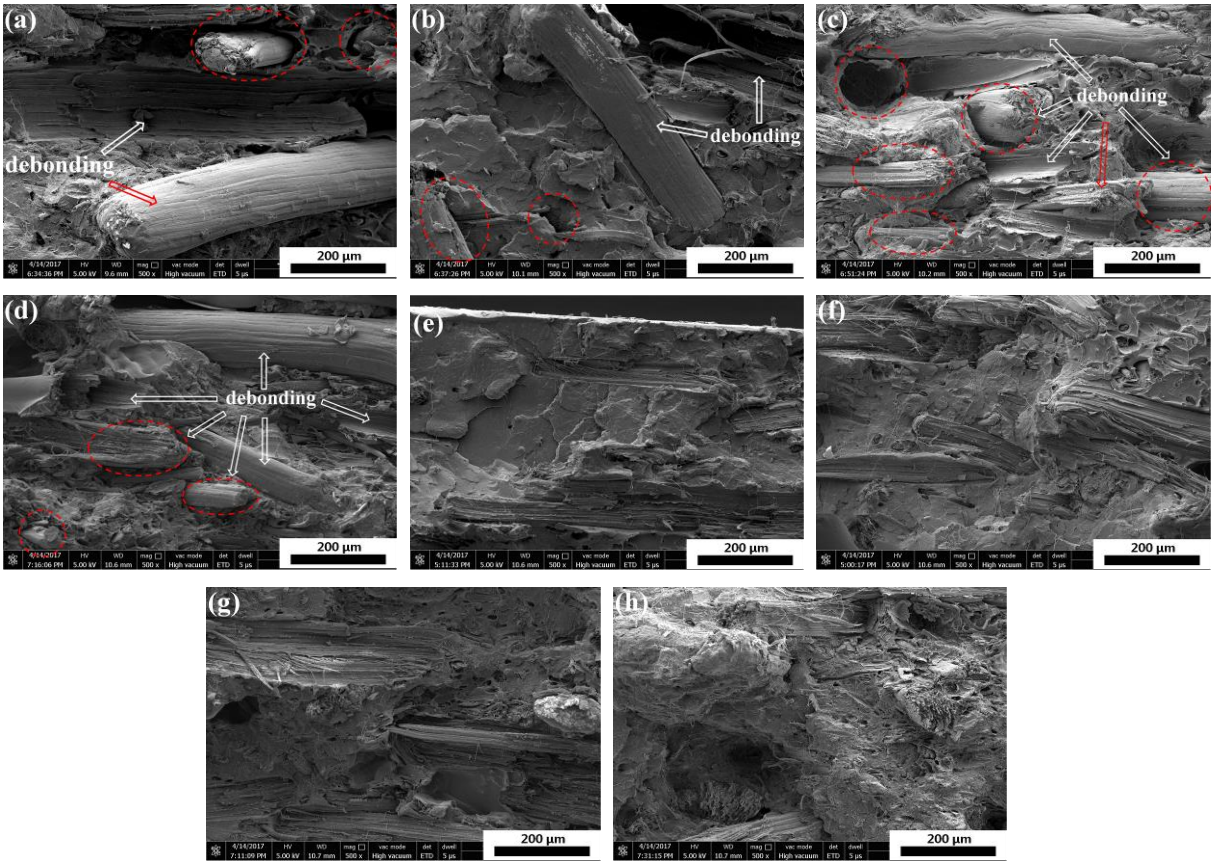

Figure 3. The tensile fracture surfaces of PLA/SF composites (90/10) (a); (80/20) (b); (70/30) (c); (60/40) (d) and PLA/SF/ADR composites (90/10/0.6) (e); (80/20/0.6) (f); (70/30/0.6) (g); (60/40/0.6) (h) with different SF content.

Many modification methods of PLA resin based on the reaction ability of the end group of PLA molecule chain, that are hydroxyl and carboxyl, by which the typical work are reaction toughening of PLA [22-26]. Considering the presence of hydroxyl on natural fiber surface, it has the possibility of bonding PLA onto sisal fiber surface by functional group reaction; therefore improving the interfacial compatibility between fibers and PLA matrix. In this study, PLA and sisal fibers were melt-blended to fabricate bio-based composites via in situ reactive interfacial compatibilization with addition of an epoxy-functionalized oligomer. Figure 4 presents the illustration of interfacial compatibilization between PLA and SF via in-situ reaction with ADR oligomer during the melt-blending processing. ADR is a kind of multi-epoxy-functionalized oligomer [19-21], which can react with end group of PLA and hydroxyl on natural fiber surface. It might bond PLA molecular onto fiber surface and play a hinge-like role between sisal fibers and PLA matrix. Therefore the addition of oligomer ADR can improve the interfacial compatibility of composites. The improved interfacial adhesion of PLA/SF/ADR composites can be observed in the above-mentioned SEM images.

Preprints (www.preprints.org) | NOT PEER-REVIEWED | Posted: 6 February 2018 doi:10.20944/preprints201802.0049.v1

Peer-reviewed version available at Materials 2018, 11, 398; doi:10.3390/ma11030398

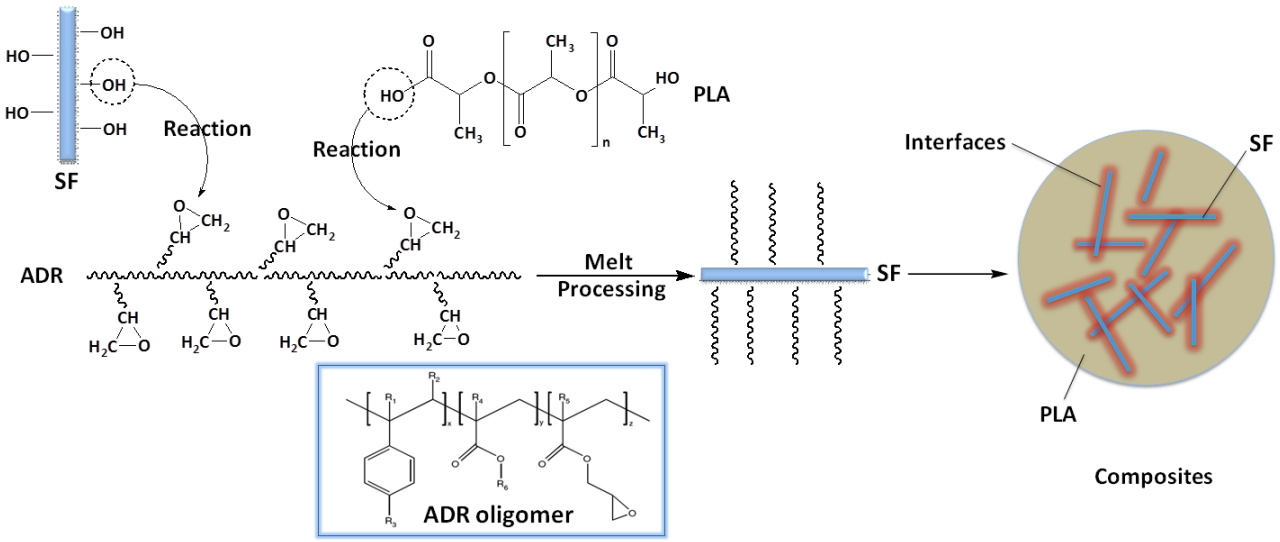

Figure 4. Illustration of interfacial compatibilization between PLA and SF via in-situ reaction with ADR oligomer during the melt-blending processing.

3.2. FTIR characterization

To demonstrate the reaction of ADR oligomer with PLA and SF, the FTIR spectra of raw SF and extracted SF from corresponding composites are shown in Figure 5. The peak at 1735 cm^{-1} stands for the stretching vibration peak of carbonyl (C=O). The bare of this 1735 cm^{-1} peak in raw SF reflected the alkaline treatment removed the lignin, impurity, pectin and waxy substances of sisal fibers [16,17]. It was also observed that no obvious 1735 cm^{-1} peak occurred in the SF extracted from PLA/SF composites, reflecting poor interfacial interaction between SF and PLA matrix in PLA/SF composites. However, it was found that the1735 cm^{-1} peak was enhanced with addition of ADR into PLA/SF composites especially for PLA/SF/ADR composites with 0.4, 0.6, and 0.8 wt% ADR addition. This phenomenon indicated the reaction of ADR oligomer with PLA and SF during the melt-blending processing, which resulted in the bonding of PLA molecular chain to sisal fibers.

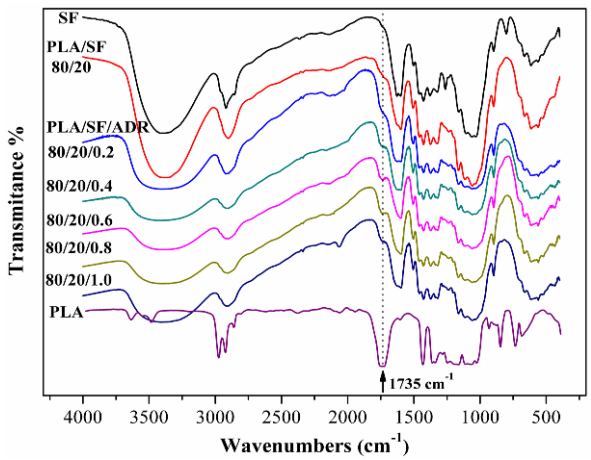

Figure 5. The FTIR spectra of raw SF, extracted SF from the composites and PLA resin.

Preprints (www.preprints.org) | NOT PEER-REVIEWED | Posted: 6 February 2018 doi:10.20944/preprints201802.0049.v1

Peer-reviewed version available at Materials 2018, 11, 398; doi:10.3390/ma11030398

3.3. DSC thermal behaviors

Figure 6a shows the DSC thermograms of PLA/SF composites and PLA/SF/ADR composites with constant 20 wt% SF and different ADR addition, from 0.2 wt% to 1.0 wt%, at the second heating scan. Cold crystallization peak and melting peak occurred in Figure 6a. At the second heating scan, as temperature elevated, the frozen PLA chain segments regain movement ability, thus the polymer obtain crystallization ability, which resulted in the presence of cold crystallization. It can be seen from Figure 6a, the cold crystallization temperature (T_{cc}) of PLA/SF/ADR composites shift to high temperature region compared with PLA/SF composites. The cold crystallization temperatures (T_{cc}) for PLA/SF and PLA/SF/ADR composites with different ADR addition were listed in Table. 2. The T_{cc} was improved with the addition of ADR oligomer, which meant that PLA/SF/ADR composites need higher temperature to regain chain segments movement ability in comparison with that of PLA/SF composites. Therefore this phenomenon demonstrated the restricted chain movement ability of PLA/SF/ADR composites [27]. This result can be ascribed to the improved interfacial interaction between PLA and SF via addition of ADR. However, the T_{cc} of PLA/SF/ADR (80/20/1.0) composites was 114.1 ℃, which was declined compared with that of PLA/SF/ADR (80/20/0,8) composites (115.5 ℃), which implied that excessive addition of ADR might be adverse to the connecting effect of ADR between SF and PLA matrix.

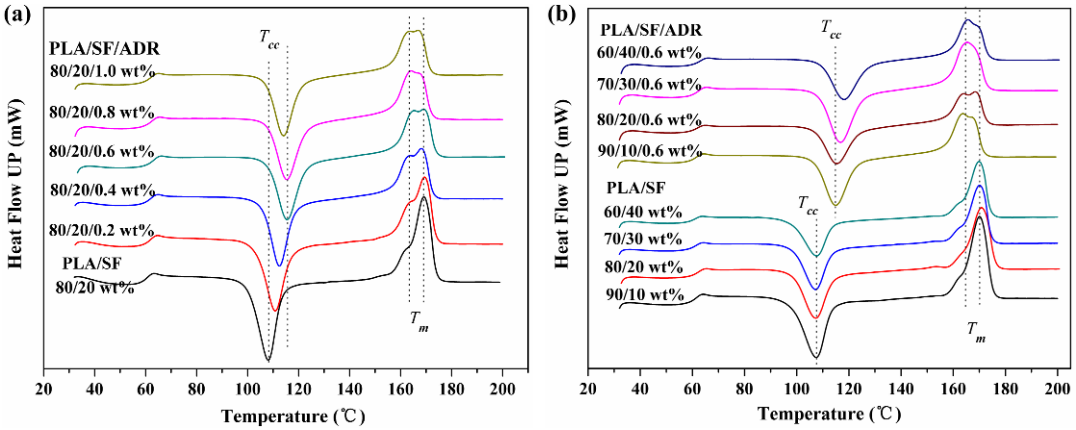

Figure 6. DSC thermograms of PLA/SF composites and PLA/SF/ADR composites with different ADR addition (a) and different SF content (b) at the second heating scan with a rate of 10 ℃/min.

Table 2. The cold crystallization temperatures (T_{cc}) for PLA/SF and PLA/SF/ADR composites with different ADR addition.

composites	PLA/SF 80/20	PLA/SF/ ADR 80/20/0.2	PLA/SF/ ADR 80/20/0.4	PLA/SF/ ADR 80/20/0.6	PLA/SF/ ADR 80/20/0.8	PLA/SF/ ADR 80/20/1.0
T_{cc} (℃)	107.7	110.8	112.1	115.7	115.5	114.1

Preprints (www.preprints.org) | NOT PEER-REVIEWED | Posted: 6 February 2018 doi:10.20944/preprints201802.0049.v1

Peer-reviewed version available at Materials 2018, 11, 398; doi:10.3390/ma11030398

At the same time, it was also found that with the addition of ADR oligomer, an obvious shoulder peak appeared in the left of melting endothermal peak (T_m 169.5 ℃) for PLA/SF/ADR composites, which indicated the formation of poor crystalline regions within PLA [28,29], corresponding to lower melting temperature. The improved interfacial interaction of PLA/SF/ADR composites resulted in restricted molecular chain movement of PLA and then more poor crystalline regions formed in the crystal growth stage, therefore a shoulder peak corresponding to lower melting temperature occurred for PLA/SF/ADR composites. The presence of shoulder peak might also be ascribed to the formation of different crystalline structures within PLA, which is transcrystallinity [15].

To further confirm theses results, Figure 6b presents the DSC thermograms of PLA/SF composites and PLA/SF/ADR composites with different SF content at the second heating scan. The cold crystallization temperatures were presented in Table 3. For PLA/SF/ADR composites, the T_{cc} increased considerably in comparison with PLA/SF composites, and an obvious shoulder peak arose in the left of melting endothermal peak. These results were consistent well with Figure 6a. At the same time, it was found that the change of SF content had little effect on T_{cc} of PLA/SF composites. However, the T_{cc} of PLA/SF/ADR composites improved with increase of SF content. For PLA/SF composites, poor interfacial interaction between SF and PLA matrix induced that more addition of SF has little effect on the movement of PLA chain segments. By contrast, for PLA/SF/ADR composites, more SF was added, more sisal fibers participated in the interfacial reaction. As a result, the improved interfacial interaction between SF and PLA matrix caused more severe restrict of PLA chain segments movement and the T_{cc} of PLA/SF/ADR composites ascended.

Table 3. The cold crystallization temperatures (T_{cc}) for PLA/SF and PLA/SF/ADR composites with different SF content.

Composites	T_{cc} (℃)	Composites	T_{cc} (℃)
PLA/SF 90/10 wt%	107.1	PLA/SF/ADR 90/10/0.6 wt%	115.4
PLA/SF 80/20 wt%	107.5	PLA/SF/ADR 80/20/0.6 wt%	115.7
PLA/SF 70/30 wt%	107.4	PLA/SF/ADR 70/30/0.6 wt%	116.9
PLA/SF 60/40 wt%	107.4	PLA/SF/ADR 60/40/0.6 wt%	117.8

The DSC thermograms of PLA/SF composites and PLA/SF/ADR composites with different ADR addition and different SF content at a cooling rate of 5℃/min are shown in Figure 7. It was found that the cooling crystallization exothermal peak declined with the addition of ADR oligomer (Figure 7a). In terms of previous analyses, the incorporating of ADR oligomer into PLA/SF composites improved the interfacial interaction between SF and PLA matrix, thus the movement of PLA segments were restricted, especially the PLA matrix

Preprints (www.preprints.org) | NOT PEER-REVIEWED | Posted: 6 February 2018 doi:10.20944/preprints201802.0049.v1

Peer-reviewed version available at Materials 2018, 11, 398; doi:10.3390/ma11030398

close to the interface. In the crystal growth stage during cooling, the moving ability of polymer segments is significant for crystallization. It can be deduced that during cooling process, no more PLA chain segments participated in cooling crystallization with the further addition of oligomer ADR because of restricted movement of PLA chain segments, therefore the crystallization of PLA/SF/ADR composites declined. The similar crystallization behaviors were found in PLA/SF composites and PLA/SF/ADR composites with different SF content (Figure 7b and Figure 7c). The cooling crystallization exothermal peaks of PLA/SF/ADR composites were significantly decreased compared with that of PLA/SF composites. At the same time, it was found that the crystallization temperature improved as SF content increased, corresponding to an enhanced crystal nucleation ability with more addition of SF. It can be attributed to the heterogeneous nucleation effect of SF.

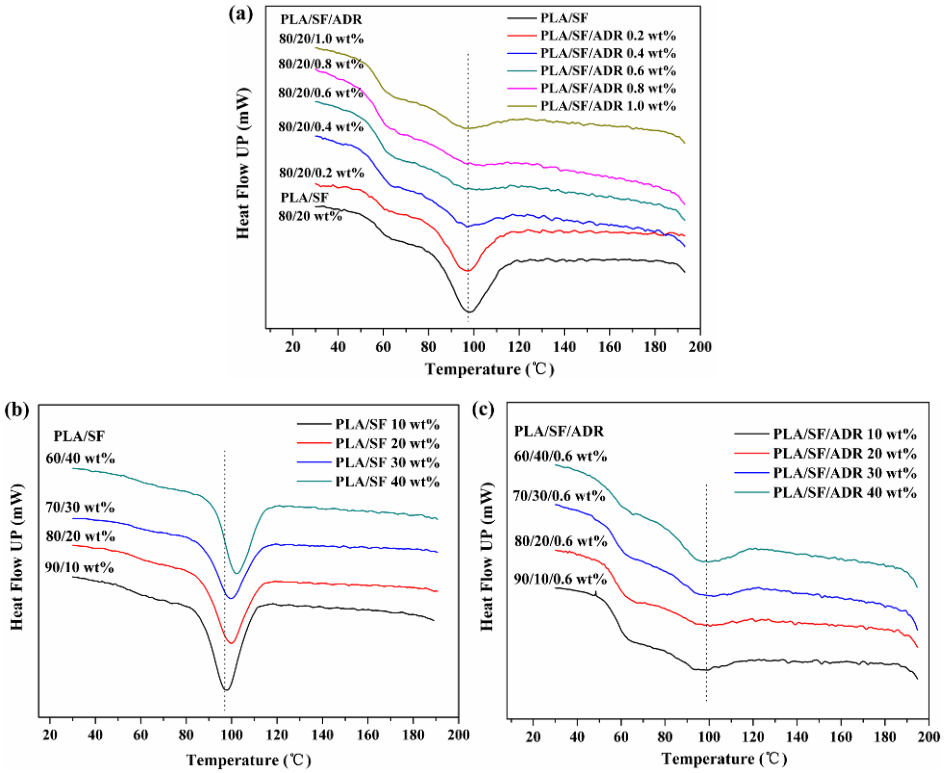

Figure 7. DSC thermograms of PLA/SF composites and PLA/SF/ADR composites with different ADR addition (a) and different SF content (b, c) at a cooling rate of 5 ℃/min.

The isothermal crystallization behavior of PLA/SF composites and PLA/SF/ADR composites were investigated at 110 ℃. Figure 8a and Figure 8b illustrate the isothermal crystallization thermograms of PLA/SF composites and PLA/SF/ADR composites with different ADR addition and different SF content at 110 ℃. The thermograms recorded heat flow (dH/dt) as a function of time. From the isothermal crystallization thermograms, the relative crystallinity as a function of crystallization time can be calculated by the following equation:

$$X_t = \frac{Q_t}{Q_\infty} = \frac{\int_0^t (dH/dt)dt}{\int_0^\infty (dH/dt)dt} \qquad (1)$$

Preprints (www.preprints.org) | NOT PEER-REVIEWED | Posted: 6 February 2018 doi:10.20944/preprints201802.0049.v1

Peer-reviewed version available at Materials 2018, 11, 398; doi:10.3390/ma11030398

Where X(t) is the relative crystallinity, and Q_∞ and Q_t are the heat generated at infinite time and at time *t*. Figure 8c and Figure 8d present the change of relative crystallinity as a function of crystallization time. To further analyze the crystallization kinetics of composites, a classic Avrami equation was used [30,31].

$$X(t) = 1 - \exp(-kt^n) \quad (2)$$

where *X(t)* is the relative crystallinity, *k* is the crystallization rate constant and *n* is the Avrami exponent reflecting the mechanisms of crystal nucleation and growth, and the following equation can be deduced from the equation (2)

$$\ln\{-\ln[1 - X(t)]\} = \ln k + n \ln t \quad (3)$$

By plotting ln［-ln(1-*X(t)*)］versus ln(*t*), the Avrami exponent, *n*, and crystallization rate constant, *k*, were determined. Meanwhile, the crystallization half-time $t_{1/2}$, reflecting the crystallization rate, can be calculated with below equation:

$$t_{1/2} = \left(\frac{\ln 2}{k}\right)^{1/n} \quad (4)$$

The obtained Avrami parameters of *n* and *k*, and calculated $t_{1/2}$ are summarized in Tab. 4 and Tab. 5.

For PLA/SF and PLA/SF/ADR composites with different ADR addition (Figure 8a), the isothermal crystallization rate decreased with the addition of ADR oligomer. As can be seen from Table 4, the crystallization half-time is 2.04 min for PLA/SF composites, and the $t_{1/2}$ increased with addition of ADR. The crystallization half-time increased to 3.99 min for composites with 0.6 wt% ADR. However, the $t_{1/2}$ tended to decrease for composites with 0.8 wt% and 1.0 wt% ADR, for which the $t_{1/2}$ were 3.09 min and 2.68 min, respectively. The calculated crystallization half-time was consistent well with the crystallization thermograms. In terms of the analyses mentioned above, the incorporation of ADR into PLA/SF composites improved the interfacial interaction between SF and PLA, but it also restricted the movement of PLA chain segment. The decline of crystallization rate of composites with addition of ADR can be credited to the restricted movement of PLA chain segment. ADR oligomer connected PLA to fiber surface via in situ reaction. However, it was found that excessive addition of ADR was adverse to the bonding effect of ADR between SF and PLA matrix. The increased crystallization rate of composites with 0.8 and 1.0 wt% ADR addition can be ascribed to the decline of bonding effect of ADR oligomer. In addition, ADR is a kind of oligomer with low molecular weight, and it might plasticize the PLA matrix in excessive addition amount, which facilitated the chain segment movement, and so improved the crystallization rate. It was found that for PLA/SF composites and PLA/SF/ADR composites with different ADR addition, the *n* value of varied from 1.954 to 2.341, reflecting that the crystals tended to grow in

Preprints (www.preprints.org) | NOT PEER-REVIEWED | Posted: 6 February 2018 doi:10.20944/preprints201802.0049.v1

Peer-reviewed version available at Materials 2018, 11, 398; doi:10.3390/ma11030398

two-dimension.

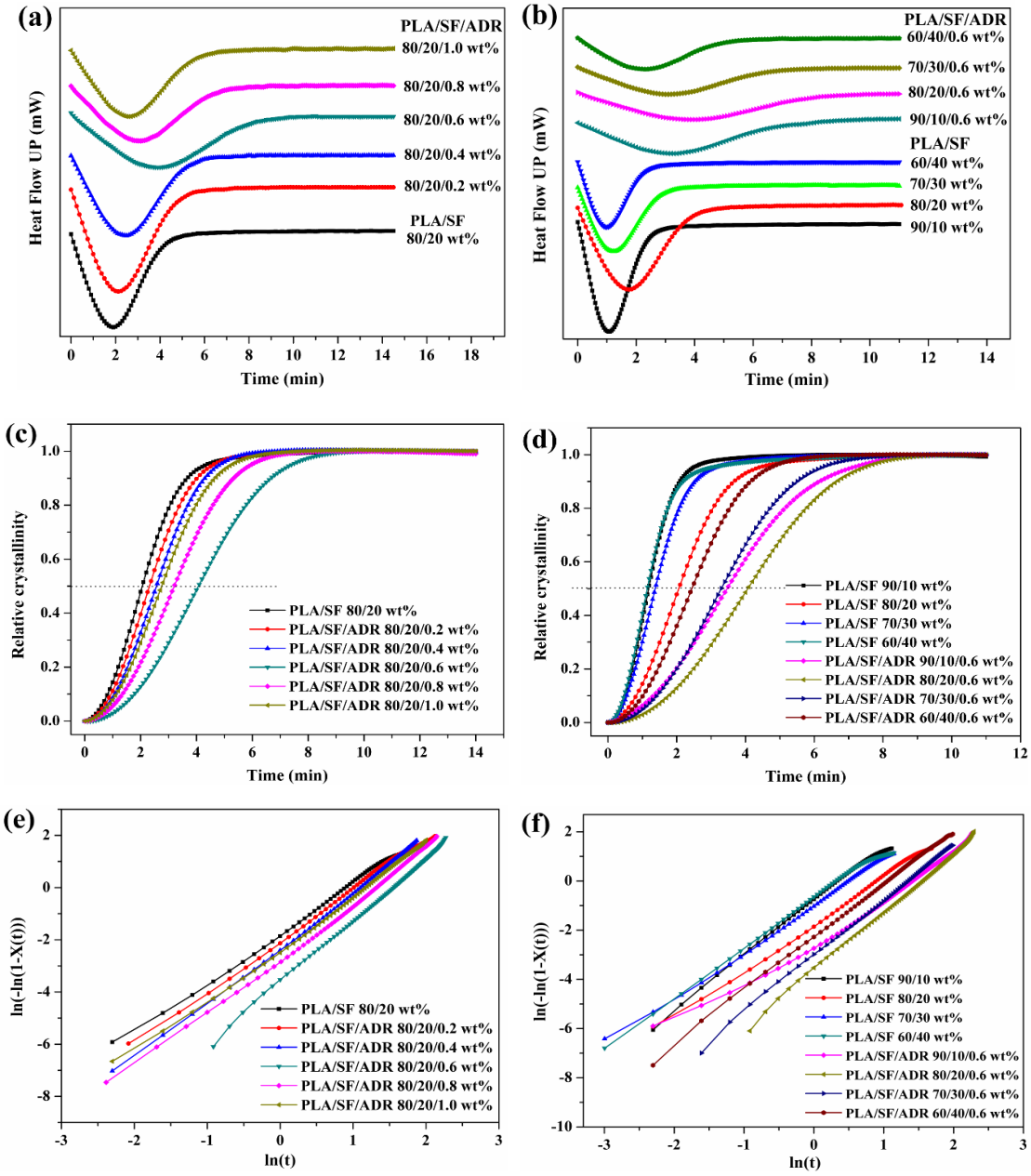

Figure 8. Isothermal crystallization of PLA/SF and PLA/SF/ADR composites: DSC thermograms (a, b), relative crystallinity (c, d) and Avrami plots (e, f).

Table 4. Isothermal crystallization half time and kinetic parameters of PLA/SF/ADR composites with different ADR addition.

samples	n	k (min^{-n})	$t_{1/2}$ (min)
PLA/SF 80/20 wt%	1.954	0.172	2.04
PLA/SF/ADR 80/20/0.2 wt%	2.030	0.139	2.21
PLA/SF/ADR 80/20/0.4 wt%	2.159	0.0965	2.49
PLA/SF/ADR 80/20/0.6 wt%	2.341	0.0272	3.99
PLA/SF/ADR 80/20/0.8 wt%	2.159	0.0604	3.09
PLA/SF/ADR 80/20/1.0 wt%	2.094	0.0879	2.68

Preprints (www.preprints.org) | NOT PEER-REVIEWED | Posted: 6 February 2018 doi:10.20944/preprints201802.0049.v1

Peer-reviewed version available at Materials 2018, 11, 398; doi:10.3390/ma11030398

For PLA/SF composites and PLA/SF/ADR composites with different SF content (Figure 8b), the similar crystallization behavior occurred. The addition of o.6 wt% ADR decreased the crystallization rate for each SF content, from 10 wt% to 40 wt%. It was also found that as increase of SF content, the crystallization half-time improved, then decrease significantly (see Table. 5). This phenomenon occurred in both PLA/SF composites and PLA/SF/ADR composites with different SF content. These results can be related to the heterogeneous nucleation effect of SF. More addition of SF restricted the movement of PLA chain segments; meanwhile it provided more heterogeneous nucleation point. The enhanced heterogeneous nucleation resulted in improving of crystallization rate of composites with high SF content, that are 30 wt% and 40 wt%.

Table 5. Isothermal crystallization half time and kinetic parameters of PLA/SF and PLA/SF/ADR composites with different SF content.

samples	n	k (min^{-n})	$t_{1/2}$ (min)
PLA/SF 90/10 wt%	2.218	0.464	1.20
PLA/SF 80/20 wt%	1.954	0.172	2.04
PLA/SF 70/30 wt%	1.933	0.373	1.38
PLA/SF 60/40 wt%	2.041	0.506	1.17
PLA/SF/ADR 90/10/0.6 wt%	1.921	0.0678	3.35
PLA/SF/ADR 80/20/0.6 wt%	2.341	0.0272	3.99
PLA/SF/ADR 70/30/0.6 wt%	2.245	0.0491	3.25
PLA/SF/ADR 60/40/0.6 wt%	2.141	0.105	2.41

3.4. Dynamic rheological behaviors

The viscoelastic response of polymers and polymers composites are very sensitive to the changes of microstructure including chain structure and phase morphology, which attracted fundamental interest in this study. Dynamic small amplitude oscillatory shear (SAOS) was performed to probe the effect of melting reactive processing with ADR oligomer on the microstructure of PLA/SF composites.

To detect the in situ reaction of composites melt, dynamic time sweep tests were performed in this study. The relative complex viscosity ($\eta^*(t)/\eta^*(0)$) versus time of PLA/SF composites and PLA/SF/ADR composites with different ADR addition are shown in Figure 9a. It was found that the complex viscosity of PLA/SF (80/20 wt%) composites decreased dramatically within time sweep because of thermal degradation. However, the presence of ADR oligomer counteracted the degradation of composites melt. The relative complex viscosity even increased at the early stage of time sweep. This phenomenon can be ascribed to the improved interfacial interaction

Preprints (www.preprints.org) | NOT PEER-REVIEWED | Posted: 6 February 2018 doi:10.20944/preprints201802.0049.v1

Peer-reviewed version available at Materials 2018, 11, 398; doi:10.3390/ma11030398

between SF and PLA matrix via in situ reaction of ADR oligomer with SF and PLA, and meanwhile the chain extension effect of ADR on PLA also contributed to the improvement of complex viscosity. Furthermore, it was found that the η*(t)/η*(0) value of PLA/ADR/ADR (80/20/0.6 wt%) composites possess the most significant improvement in the early stage of time sweep. This results was consistent well with the analyses mentioned above. Excessive addition of ADR oligomer, more than 0.6 wt% content, was not facilitated to improve the interfacial interaction of composites.

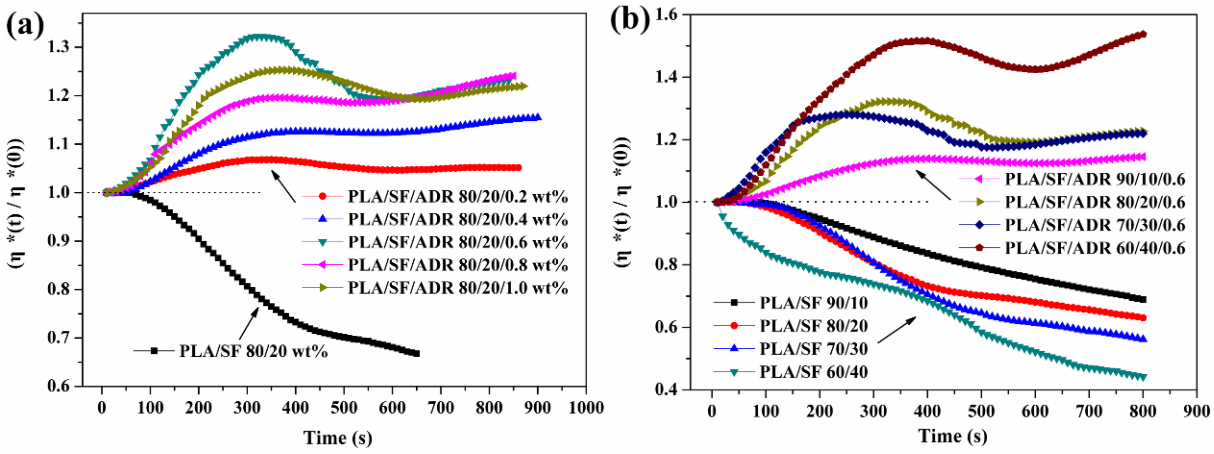

Figure 9. Relative complex viscosity (η*(t)/η*(0)) versus time of PLA/SF and PLA/SF/ADR composites with different ADR addition (a) and different SF content (b).

Figure 9b shows the relative complex viscosity (η*(t)/η*(0)) versus time of PLA/SF composites and PLA/SF/ADR composites with different SF content. For PLA/SF composites with different SF content, the complex viscosity declined severely within time sweep. The addition of 0.6 wt% ADR oligomer can effectively inhibited the reduction of complex viscosity of composites. As can be seen from Figure 10b, the η*(t)/η*(0) value of PLA/SF/ADR composites tended to be enhanced within the time sweep. Furthermore, it was found that for PLA/SF composites, the more the SF was added, the more the η*(t)/η*(0) value would decrease. That is because the presence of SF aggravated the thermal degradation of composites. However, for PLA/SF/ADR composites with 0.6 wt% ADR oligomer, the η*(t)/η*(0) value of composites ascend with the SF content increase because more SF addition could result in more SF participating in the interfacial reaction and improve the interfacial interaction between SF and PLA matrix. The PLA/SF/ADR (60/40/0.6 wt%) composites exhibited most significantly improvement in the η*(t)/η*(0) value.

Preprints (www.preprints.org) | NOT PEER-REVIEWED | Posted: 6 February 2018 doi:10.20944/preprints201802.0049.v1

Peer-reviewed version available at Materials 2018, 11, 398; doi:10.3390/ma11030398

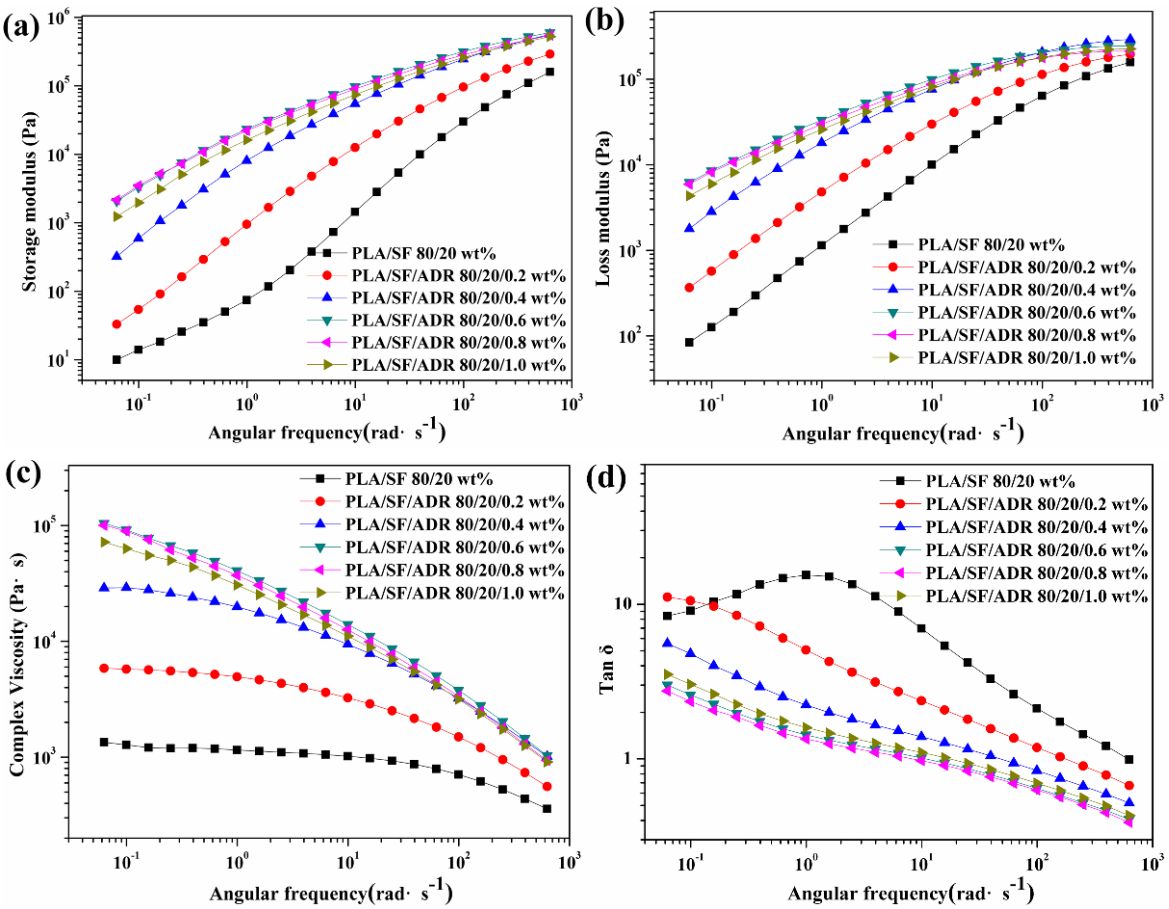

Figure 10. Changes of storage modulus (a), loss modulus (b), complex viscosity $|\eta^*|$ (c) and tan δ (d) as functions of angular frequency for PLA/SF and PLA/SF/ADR composites with different ADR addition.

The changes of storage modulus (G′), loss modulus (G″), complex viscosity $|\eta^*|$ and loss tangent as functions of angular frequency for PLA/SF and PLA/SF/ADR composites with different ADR addition are shown in Figure 10. It can be seen from Figure 10a and Figure 10b, the addition of ADR oligomer improved the storage modulus and loss modulus of PLA/SF composites. It reflects enhanced viscoelastic response of PLA/SF/ADR composites compared with that of PLA/SF composites. Figure 10c presents the changes of complex viscosity as a function of angular frequency. It can be seen that the complex viscosity improved with addition of ADR oligomer, especially at the low angular frequency region. In addition, the pattern of dependence of complex viscosity on frequency (the change tendency of complex viscosity with frequency) varied to some extent due to the addition of ADR. For PLA/SF composites and PLA/SF/ADR composites with low ADR content, 0.2 wt% and 0.4 wt%, the complex viscosity nearly keep constant at the low angular frequency region, and then decreased angular frequency increased. This appearance that transition from Newtonian plateau to power law regime at the inflection point, is a typical phenomenon of polymer materials. However it was found that the Newtonian plateau region decreased with the addition of ADR oligomer. For composites with high ADR

Peer-reviewed version available at Materials 2018, 11, 398; doi:10.3390/ma11030398

content, that were 0.6 wt%, 0.8 wt%, and 1.0 wt%, the shear-thinning behavior occurred in the whole angular frequency region, which exhibited more obviously power law regime [32,33]. The enhanced shear-thinning behavior of PLA/SF/ADR composites can be ascribed to the improved interfacial interaction of composites. For PLA/SF/ADR composites, which the interfacial interaction between SF and PLA matrix were enhanced, the sisal fibers can act as physical crossing points in composites melt. Therefore, it can be deduced that more significant disentanglement of polymer chain occurred as the angular frequency increased, resulted in more obvious shear-thinning behavior than that of PLA/SF composites. Figure 10d presents the changes of loss tangent (tan δ = G″/G′) as a function of angular frequency. It can be seen that the tan δ of PLA/SF/ADR composites decreased in compared with that of PLA/SF composites. The PLA/SF/ADR composites possess more dramatically elastic response. The frequency dependence of loss tangent can be used to characterize the gel point of cross-linking system [34,35]. This method can be adopted for polymer composites to evaluate the percolation thresholds of the fillers [36,37]. The tan δ of PLA/SF/ADR composites displayed less dependence on angular frequency, which exhibited a gel-like behavior. In terms of the analyses mentioned above, the presence of ADR improved interfacial interaction of composites, and sisal fibers physical crossing points in composites melt. Therefore, the stress relaxation of PLA molecular chain became more difficult in the melt state; the elastic response of PLA/SF/ADR composites melt enhanced and tended to exhibit a gel-like behavior.

3.5. DMA characterization

In order to evaluate the dynamic mechanical properties and investigate the effect of ADR on the glass transition of composites, the DMA measurements of PLA/SF composites and PLA/SF/ADR composites with different SF content were carried out at different frequencies. Effect of different frequencies on loss tangent (tan δ) of PLA/SF and PLA/SF/ADR composites with different SF content with a heating rate of 2 ℃/min is shown in Figure 11. It was observed that in the whole temperature range the α relaxation for PLA/SF and PLA/SF/ADR composites was between 60 ℃ to 70 ℃ which corresponds to the glass transition temperature (T_g) of composites. The glass transition temperature of composites was summarized in Table 6. The T_g of composites increased as frequencies elevated. It was found that the T_g of PLA/SF/ADR composites was improved compared with that of PLA/SF composites at the identical test frequencies, which demonstrated that the moving ability of PLA chain segments were restrained. This result confirmed the enhanced interfacial interaction between SF and PLA matrix via in situ interfacial reaction.

Preprints (www.preprints.org) | NOT PEER-REVIEWED | Posted: 6 February 2018 doi:10.20944/preprints201802.0049.v1

Peer-reviewed version available at Materials 2018, 11, 398; doi:10.3390/ma11030398

Table 6. The glass transition temperature of PLA/SF composites and PLA/SF/TGIC composites with different ADR addition at different frequency on tan δ.

samples		0.1 (HZ)	0.5 (HZ)	1 (HZ)	5 (HZ)	20 (HZ)
PLA/SF 90/10 wt %		58.6	62.0	62.9	64.9	67.9
PLA/SF/ADR 90/10/0.6 wt %		61.8	63.2	64.6	67.9	69.9
PLA/SF 80/20 wt %		61.1	62.9	63.4	67.0	69.4
PLA/SF/ADR 80/20/0.6 wt %	T_g(℃)	61.3	62.9	64.6	67.5	68.95
PLA/SF 70/30 wt %		61.2	63.0	63.1	66.4	68.9
PLA/SF/ADR 70/30/0.6 wt %		60.7	63.1	63.6	66.5	68.4
PLA/SF 60/40 wt %		60.2	61.9	62.5	65.9	67.5
PLA/SF/ADR 60/40/0.6 wt %		61.0	62.7	63.2	66.1	67.8

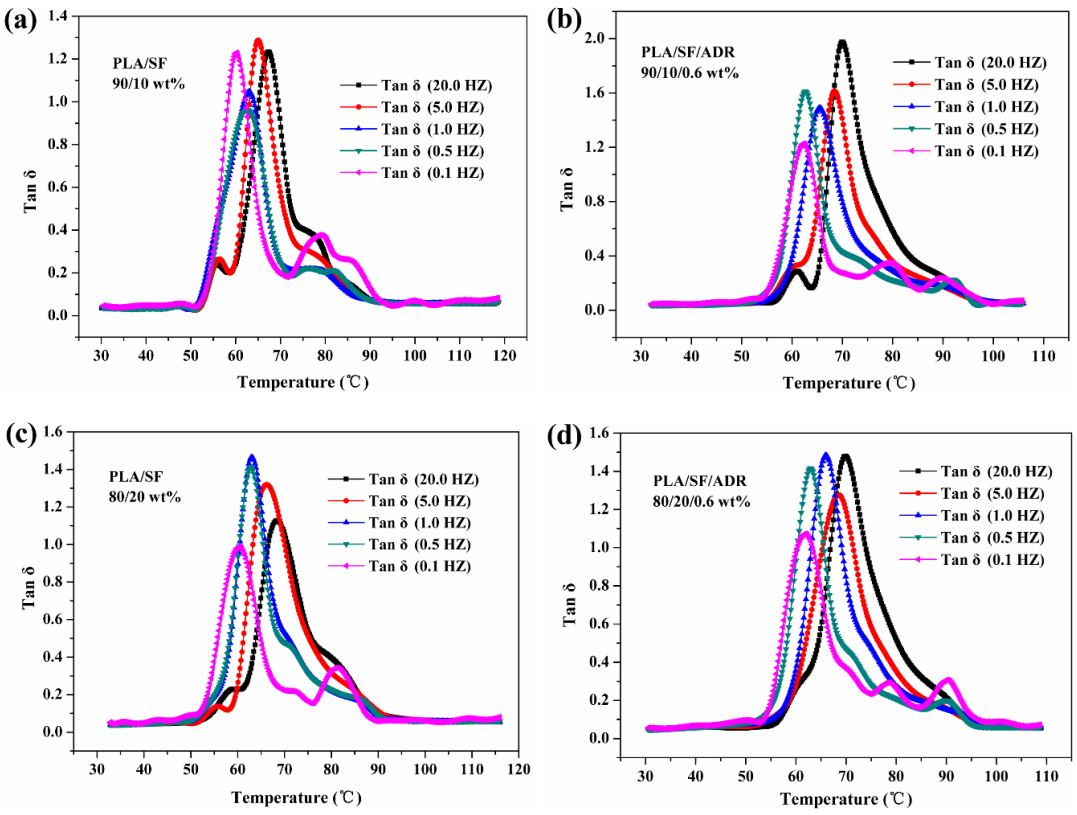

Preprints (www.preprints.org) | NOT PEER-REVIEWED | Posted: 6 February 2018 doi:10.20944/preprints201802.0049.v1

Peer-reviewed version available at Materials 2018, 11, 398; doi:10.3390/ma11030398

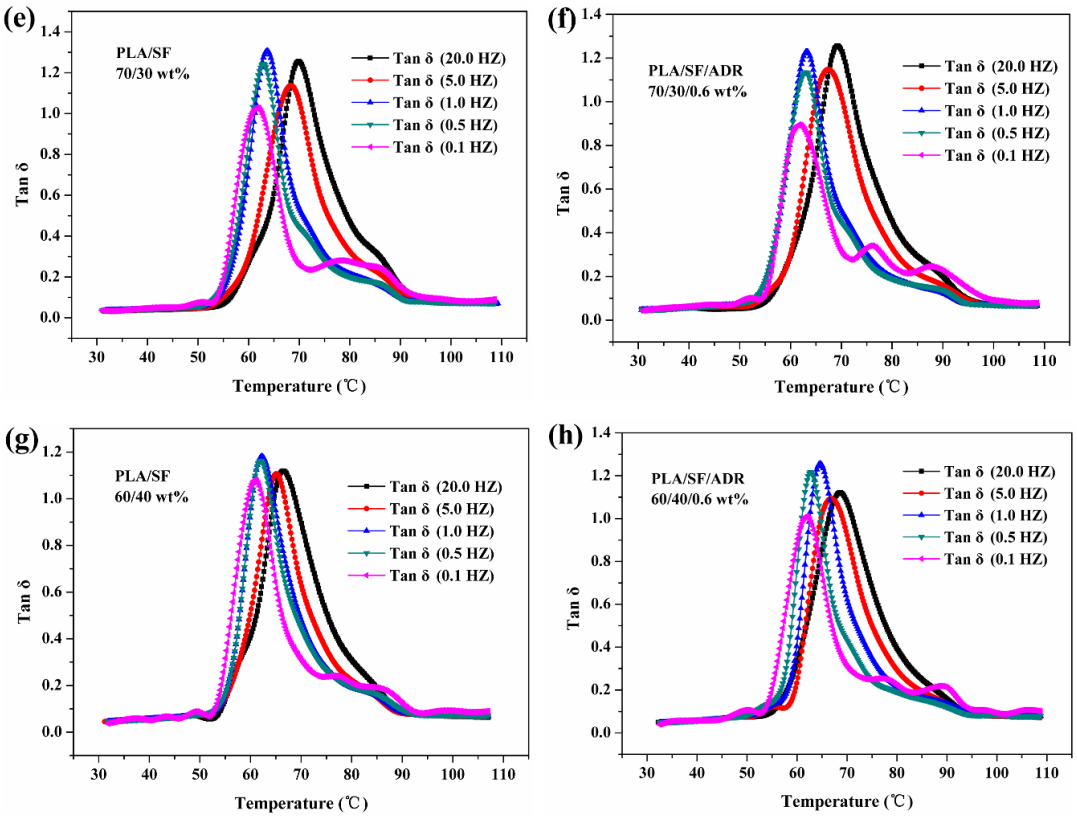

Figure 11. Effect of different frequencies on tan δ of PLA/SF and PLA/SF/ADR composites with different SF content at a heating rate of 2 ℃/min.

To further analysis the glass transition of composites, the activation energies of glass transition relaxation (ΔE_a) were calculated based on the dependence of T_g on frequencies. The ΔE_a represents the energy barrier of glass transition relaxation. It can be adopted to characterize the relationship between polymer chain segment mobility and the time scale. Five different test frequencies were used in this study (0.1, 0.5, 1, 5 and 20 HZ). The changes of glass transition temperature were interrelated with test frequencies using the Arrhenius equation [38,39].On the basis of classic Arrhenius equation, the molecular relaxation time can be expressed as:

$$\tau = \tau_0 e^{\frac{\Delta E - \gamma\sigma}{RT}} \quad (5)$$

where ΔE and σ are the activation energy of relaxation and the stress, respectively, τ_0 is the hypothetical relaxation time at an infinite temperature, T is the absolute temperature, γ is the variable and R is the gas constant.

Here, the stress (σ) is small, thus equation (5) can be simplified as:

$$\tau = \tau_0 e^{\frac{\Delta E}{RT}} \quad (6)$$

$$\ln \tau = \ln \tau_0 + \frac{\Delta E}{RT} \quad (7)$$

Preprints (www.preprints.org) | NOT PEER-REVIEWED | Posted: 6 February 2018 doi:10.20944/preprints201802.0049.v1

Peer-reviewed version available at Materials 2018, 11, 398; doi:10.3390/ma11030398

The relaxation times were calculated from the relationship:

$$\tau = \frac{1}{f} \tag{8}$$

A combination of equation (7) and (8) leads to:

$$\ln f = -\ln \tau_0 - \frac{\Delta E}{RT} \tag{9}$$

According to equation (9), a plot of ln *f versus 1/T* should give a straight line with a slope that is proportional to activation energy associated to the glass transition relaxation. Figure 12 shows the Arrhenius plots of relaxation times versus 1/T, the respective linear fits of PLA/SF composites and PLA/SF/ADR composites with different SF content, and the calculated activation energies of glass transition relaxation. As can be seen from Table 7 and Figure 12c, the calculated ΔE_a of composites increased with the addition of ADR oligomer at the identical SF content, which implied that the improved interfacial adhesion of composites increased the energy barrier of the mobility of the PLA chain segments. In addition, for both PLA/SF composites and PLA/SF/ADR composites, the ΔE_a value increased with SF content uprise. Furthermore, the improvement of activation energy of PLA/SF/ADR composites compared with that of PLA/SF composites at the identical SF content was elevated as more SF content (see Figure 12c). The more addition of SF, the more sisal fibers participated in interfacial reaction, resulted in more significantly restrict of PLA chain segments. These results paralleled well with the thermal and rheological analyses mentioned above.

Table 7. The calculated activation energies of glass transition relaxation for PLA/SF composites and PLA/SF/ADR composites with different SF content.

Samples	PLA/SF 90/10	PLA/SF 80/20	PLA/SF 70/30	PLA/SF 60/40	PLA/SF/ ADR 90/10/0.6	PLA/SF/ ADR 80/20/0.6	PLA/SF/ ADR 70/30/0.6	PLA/SF/ ADR 60/40/0.6
ΔE_a (KJ/mol)	557.21	578.37	597.82	621.40	581.02	611.28	655.52	716.76

Preprints (www.preprints.org) | NOT PEER-REVIEWED | Posted: 6 February 2018 doi:10.20944/preprints201802.0049.v1

Peer-reviewed version available at Materials 2018, 11, 398; doi:10.3390/ma11030398

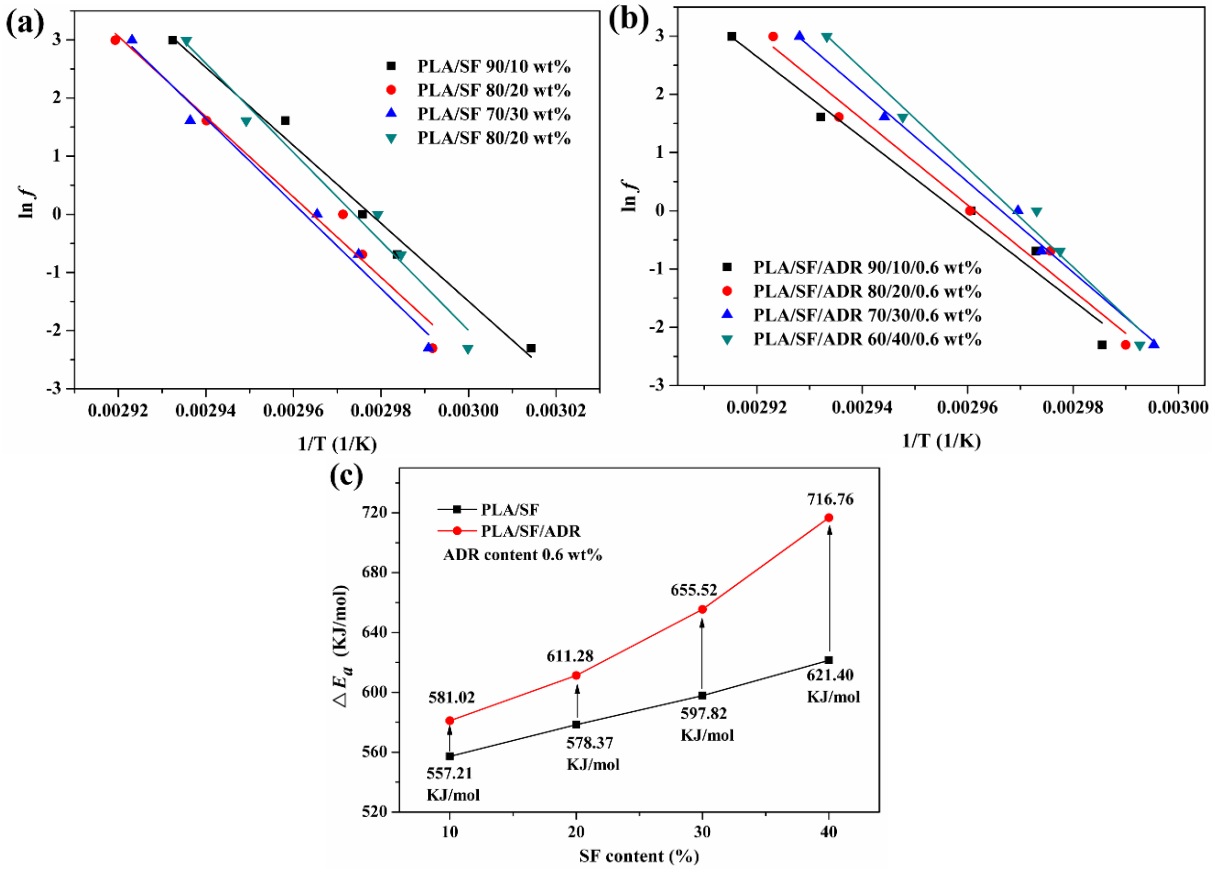

Figure 12. Arrhenius plots of relaxation times versus 1/T and the respective linear fits of PLA/SF composites (a) and PLA/SF/ADR composites (b) with different SF content and the calculated activation energies (ΔE_a) of glass transition relaxation (c).

3.6. Mechanical properties

Figure 13 shows the tensile properties and impact strength of PLA/SF composites and PLA/SF/ADR composites with different ADR addition. It was found that the addition of ADR oligomer improved the tensile strength of composites (Figure 13a). Moreover, as the increase of ADR content, the tensile strength of PLA/SF/ADR composites ascended at first and then decreased. The PLA/SF/ADR (80/20/0.6 wt%) composites possessed the highest tensile strength. The similar variation tendency occurred for tensile modulus of composites, which reflected the enhanced stiffness of PLA/ADR/SF composites compared with that of PLA/SF composites. Furthermore, it was found that the elongation at break and the impact strength of PLA/SF/ADR composite was improved in comparison with that of PLA/SF composites (Figure 13b), which indicated an enhanced toughness of composites with addition of ADR oligomer. These results demonstrated that the incorporating of ADR oligomer simultaneously reinforce and toughen the PLA/SF composites. Figure 14 shows the tensile properties and impact strength of PLA/SF composites and PLA/SF/ADR composites with different SF content. For PLA/SF composites, the tensile strength decreased as SF content increased. However, for PLA/SF/ADR composites with 0.6 wt% ADR oligomer, the tensile strength improved with the increase of SF content, exhibiting the more

Preprints (www.preprints.org) | NOT PEER-REVIEWED | Posted: 6 February 2018 doi:10.20944/preprints201802.0049.v1

Peer-reviewed version available at Materials 2018, 11, 398; doi:10.3390/ma11030398

addition of SF the more significantly improvement of tensile strength compared with that of PLA/SF composites at the identical SF content (Figure 14a). In addition, the tensile modulus of PLA/SF and PLA/SF/ADR composites were enhanced with high SF content, and the elevation of tensile modulus became more significantly at higher SF content. Figure 14b presents that the elongation at break of composites decrease with the increase of SF content, and at the identical SF content the elongation at break is improved via addition of ADR oligomer. The impact strength of PLA/SF/ADR composites with different SF content was also improved in comparison with that of PLA/SF composites (see Figure 14c).

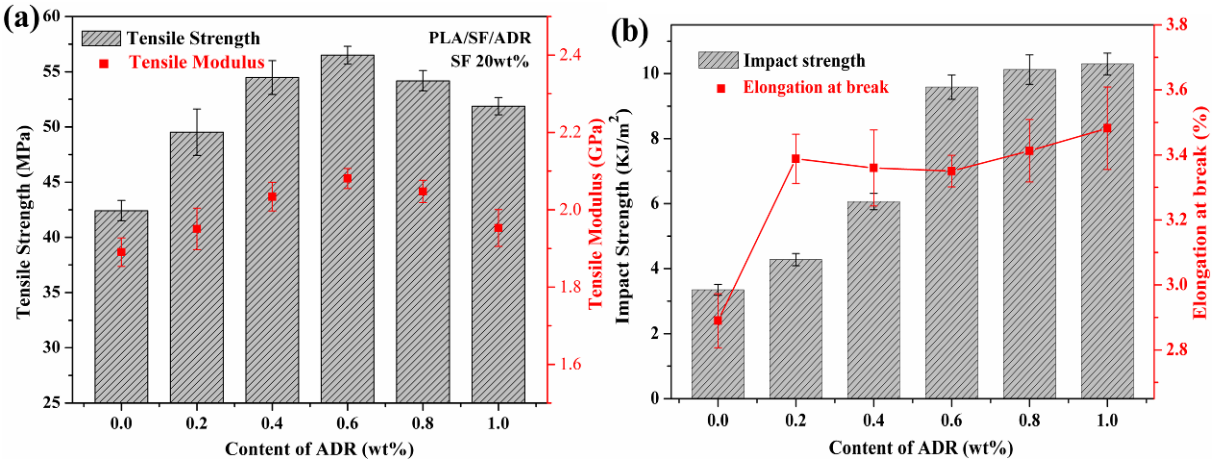

Figure 13. Tensile strength (a), tensile modulus (a), elongation at break (b) and impact strength (b) of PLA/SF/ADR composites with different ADR addition and constant 20 wt% SF content.

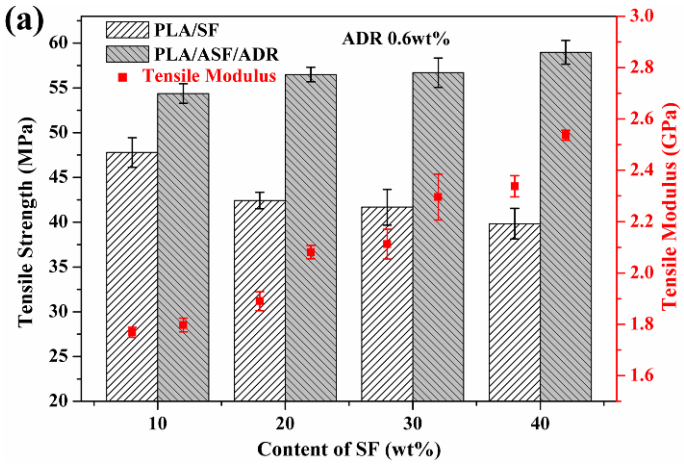

Preprints (www.preprints.org) | NOT PEER-REVIEWED | Posted: 6 February 2018 doi:10.20944/preprints201802.0049.v1

Peer-reviewed version available at Materials 2018, 11, 398; doi:10.3390/ma11030398

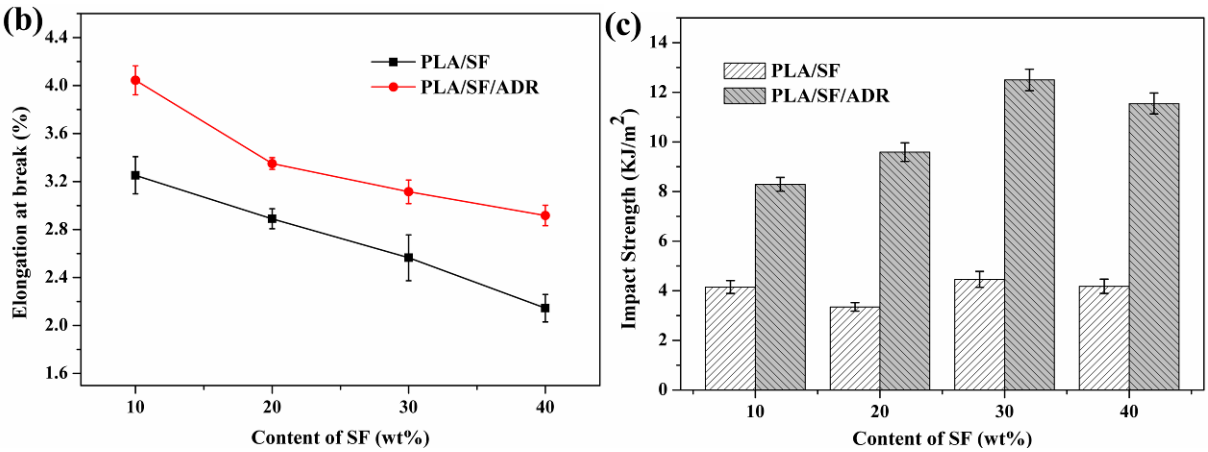

Figure 14. Tensile strength (a), tensile modulus (a), elongation at break (b) and impact strength (c) of PLA/SF and PLA/SF/ADR composites with different SF content and constant 0.6 wt% ADR addition.

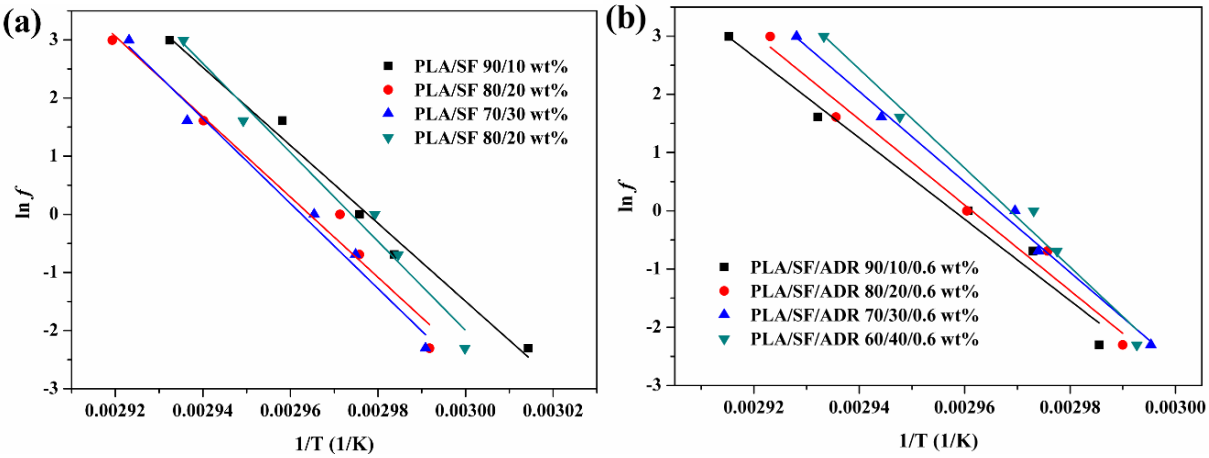

In brief, when the fiber reinforced plastic is bearing force, the role of interface is transmitting stress from polymer matrix to fibers; therefore the mechanical properties of PLA/SF composites in this study were significantly influenced by fiber-matrix interaction [40]. According to the microstructure characterization and analyses mentioned above, the addition of ADR oligomer improved the interfacial adhesion of PLA/SF composites via in-situ interfacial reaction during melt-blending and processing. The improved interfacial interaction of PLA/SF composites enhanced the efficiency of transmitting stress from PLA matrix to sisal fibers, thus improved the mechanical properties. However, excessive addition of ADR was adverse to the connecting effect of ADR between SF and PLA matrix, which not facilitated the enhancement of interfacial adhesion. Therefore PLA/SF/ADR composites with high ADR addition, that were 0.8 wt% and 1.0 wt% in this study, slightly decreased compared with composites with 0.6 wt% ADR. At the same time, ADR is a kind of oligomer with low molecular weight and flexible chain compared with PLA. It had a plasticize effect on PLA matrix, which also contributed to the toughening of composites.

At the same time, poorer interfacial adhesion resulted in more microstructure defect of composites (see Figure

2), and caused in more stress concentration point in bearing force, which was bad for the mechanical properties of composites. Improving interfacial interaction between SF and PLA matrix contributed to formation of moderate interface in composites. A moderate interface can effectively relieve the stress concentration under loading conditions, and make the stress transmitting uniformly from matrix to fibers [41,42]. For PLA/SF composites with different SF content, the more addition of sisal fibers the more microstructure defect presence in composites, resulted in a decline of mechanical properties of PLA/SF composites as increased of SF content. By contrast, the mechanical properties of PLA/SF/ADR composites were improved because of enhanced interfacial adhesion of composites via in situ reactive interfacial compatibilization with addition of ADR oligomer.

4. Conclusions

In this study, polylactide/sisal fibers biocomposites was fabricated using a simple in situ reactive melt-blending method with addition of an epoxy-functionalized oligomer. ADR oligomer played a hinge-like role between sisal fibers and PLA matrix via in situ interfacial reaction with SF and PLA during melt blending and processing, resulted in improved interfacial interaction between SF and PLA matrix. SEM morphology characterization confirmed the improved interfacial adhesion of PLA/SF/ADR composites, and FTIR analysis demonstrated the bonding of PLA molecular chain with SF in composites. The effect of in situ reaction with ADR oligomer on thermal and rheological of PLA/SF composites was investigated. The results indicated that the crystallization ability of composites declined and the viscoelastic response was enhanced via addition of ADR. In turn, these results further reflected the restricted mobility of PLA molecular chain or segments because of enhanced interfacial interaction between SF and PLA matrix via interfacial reaction with ADR oligomer. These results were further demonstrated by the activation energies of glass transition relaxation (ΔE_a) of composites, which were calculated via dynamic mechanical analysis. The tensile properties and impact strength of composites were improved because of improved interfacial compatibility, which demonstrated that the incorporating of ADR oligomer can simultaneously reinforce and toughening the PLA/SF composites.

Acknowledgments

This work was financial supported by the Specialized Research Fund for the Doctoral Program of Higher Education of China (20120172130004), the National Key Research and Development Program of China (Grant No. 2016YFB0302301) and Key Program of National Natural Science Foundation of China (Grant No. 51435005).

References

[1] Cicala, G.; Tosto, C.; Latteri, A.; Blanco, L.; Elsabbagh, A.; Russo, P.; Ziegmann, G. Green Composites Based on Blends of Polypropylene with Liquid Wood Reinforced with Hemp Fibers: Thermomechanical

Properties and the Effect of Recycling Cycles. *Materials* **2017**, 10, 998-1014.

[2] Gurunathan, T.; Mohanty, S.; Nayak, S.K. A review of the recent developments in biocomposites based on natural fibres and their application perspectives. *Composites Part A Applied Science & Manufacturing* **2015**, 77, 1-25.

[3] Pickering, K.L.; Efendy, M.G.A.; Le, T.M. A review of recent developments in natural fibre composites and their mechanical performance. *Composites Part A Applied Science & Manufacturing* **2016**, 83, 98-112.

[4] Liu, W.; Xie, T.; Qiu, R. N-methylol acrylamide grafting bamboo fibers and their composites. *Composites Science & Technology* **2015**, 117, 100-106.

[5] Tran, L.Q.N.; Fuentes, C.A.; Dupont-Gillain, C. Understanding the interfacial compatibility and adhesion of natural coir fibre thermoplastic composites. *Composites Science & Technology* **2013**, 80, 23-30.

[6] Sipião, B.L.S.; Reis, L.S.; Paiva, R.D.L.M.; Capri, M.R.; Mulinari, D.R. Interfacial Adhesion in Natural Fiber-Reinforced Polymer Composites. In *Lignocellulosic Polymer Composites: Processing, Characterization and Properties*.; Petinakis., Eds.; Wiley, New York, **2014**; pp. 17-39.

[7] Faruk, O.; Bledzki, A.K.; Fink, H.P. Biocomposites reinforced with natural fibers: 2000-2010. *Progress in Polymer Science* **2012**, 37, 1552-1596.

[8] Kabir, M.M.; Wang, H.; Lau, K.T. Chemical treatments on plant-based natural fibre reinforced polymer composites: An overview. *Composites Part B Engineering* **2012**, 43, 2883-2892.

[9] Xie, Y.; Hill, C.A.S.; Xiao, Z. Silane coupling agents used for natural fiber/polymer composites: A review. *Composites Part A Applied Science & Manufacturing* **2010**, 41, 806-819.

[10] Nishitani, Y.; Kajiyama, T.; Yamanaka, T. Effect of Silane Coupling Agent on Tribological Properties of Hemp Fiber-Reinforced Plant-Derived Polyamide 1010 Biomass Composites. *Materials* **2017**, 10, 1040-1061.

[11] Bledzki, A.K.; Mamun, A.A.; Lucka-Gabor, M.; Gutowski, V.S. The effects of acetylation on properties of flax fibre and its polypropylene composites. *Express Polymer Letters* **2008**, 2, 413-422.

[12] Wang, B.; Panigrahi, S.; Tabil, L. Pre-treatment of Flax Fibers for use in Rotationally Molded Biocomposites. *Journal of Reinforced Plastics & Composites* **2007**, 26, 447-463.

[13] Zahran, M.K.; Rehan, M.F. Grafting of acrylic acid onto flax fibers using Mn(IV)-citric acid redox system. *Journal of Applied Polymer Science* **2006**, 102, 3028-3036.

[14] Kalia, S.; Kaith, B.S.; Kaur, I. Pretreatments of natural fibers and their application as reinforcing material in polymer composites—A review. *Polymer Engineering & Science* **2009**, 49, 1253–1272.

[15] Zhou, M.; Li, Y.; He, C. Interfacial crystallization enhanced interfacial interaction of Poly (butylene succinate)/ramie fiber biocomposites using dopamine as a modifier. *Composites Science & Technology* **2014**, 91, 22-29.

[16] Sgriccia, N.; Hawley, M.C.; Misra, M. Characterization of natural fiber surfaces and natural fiber composites. *Composites Part A Applied Science & Manufacturing* **2008**, 39, 1632-1637.

[17] Farahani, G.N.; Ahmad, I.; Mosadeghzad, Z. Effect of Fiber Content, Fiber Length and Alkali Treatment on Properties of Kenaf Fiber/UPR Composites Based on Recycled PET Wastes. *Polymer-Plastics Technology and Engineering* **2012**, 51, 634-639.

[18] Sipião, B.L.S.; Reis, L.S.; Paiva, R.D.L.M.; Capri, M.R.; Mulinari, D.R. Chemical Modification and Properties of Cellulose-Based Polymer Composites. In *Lignocellulosic Polymer Composites: Processing, Characterization and Properties*.; Petinakis., Eds.; Wiley, New York, **2014**; pp. 301-323.

[19] Villalobos, M.; Awojulu, A.; Greeley, T. Oligomeric chain extenders for economic reprocessing and recycling of condensation plastics. *Energy* **2006**, 31, 3227-3234.

[20] Al-Itry, R.; Lamnawar, K.; Maazouz, A.; Billon, N.; Combeaud, C. Effect of the simultaneous biaxial stretching on the structural and mechanical properties of PLA, PBAT and their blends at rubbery state. *European Polymer Journal* **2015**, 68, 288-301.

[21] Arruda, L.C.; Magaton, M.; Bretas, R.E.S.; Ueki, M.M. Influence of chain extender on mechanical, thermal and morphological properties of blown films of PLA/PBAT blends. *Polymer Testing* **2015**, 43, 27-37.

[22] Liu, H.; Song, W.; Chen, F. Interaction of Microstructure and Interfacial Adhesion on Impact Performance of Polylactide (PLA) Ternary Blends. *Macromolecules* **2011**, 44, 1513-1522.

[23] Zhang, K.; Nagarajan, V.; Misra, M. Supertoughened Renewable PLA Reactive Multiphase Blends System: Phase Morphology and Performance. *Acs Applied Materials & Interfaces* **2014**, 6, 12436-12448.

[24] Ojijo, V.; Ray, S.S. Super toughened biodegradable polylactide blends with non-linear copolymer interfacial architecture obtained via facile in-situ reactive compatibilization. *Polymer* **2015**, 80, 1-17.

[25] Wu, M.; Wu, Z.; Wang, K. Simultaneous the thermodynamics favorable compatibility and morphology to achieve excellent comprehensive mechanics in PLA/OBC blend. *Polymer* **2014**, 55, 6409-6417.

[26] Hao, M.; Wu, H.; Zhu, Z. In situ reactive interfacial compatibilization of polylactide/sisal fiber biocomposites via melt-blending with an epoxy-functionalized terpolymer elastomer. *Rsc Advances* **2017**, 7, 32399-32412.

[27] Xiong, Z.; Yang, Y.; Feng, J. Preparation and characterization of poly(lactic acid)/starch composites toughened with epoxidized soybean oil. *Carbohydrate Polymers* **2013**, 92, 810-816.

[28] Cartier, L.; Okihara, T.; Ikada Y. Epitaxial crystallization and crystalline polymorphism of polylactides. *Polymer* **2000**, 41, 8909-8919.

[29] Martin, O.; Avérous, L. Poly(lactic acid): plasticization and properties of biodegradable multiphase systems. *Polymer* **2001**, 42, 6209-6219.

[30] Avrami, M. Kinetics of Phase Change. I General Theory. *Journal of Chemical Physics* **1939**, 7, 1103-1112.

[31] Avrami, M. Kinetics of Phase Change. II Transformation-Time Relations for Random Distribution of Nuclei. *Journal of Chemical Physics* **1940**, 8, 212-224.

[32] Xu, H.; Fang, H.; Bai, J.; Zhang, Y.; Wang, Z. Preparation and Characterization of High-Melt-Strength

Polylactide with Long-Chain Branched Structure through γ-Radiation-Induced Chemical Reactions. *Industrial & Engineering Chemistry Research* **2014**, 53, 1150-1159.

[33] Fang, H.; Jiang, F.; Wu, Q. Supertough polylactide materials prepared through in situ reactive blending with PEG-based diacrylate monomer. *Acs Applied Materials & Interfaces* **2014**, 6, 13552-13563.

[34] Winter, H.H.; Chambon, F. Analysis of Linear Viscoelasticity of a Crosslinking Polymer at the Gel Point. *Journal of Rheology* **1986**, 30, 367-382.

[35] Chambon, F.; Winter, H.H. Linear Viscoelasticity at the Gel Point of a Crosslinking PDMS with Imbalanced Stoichiometry. *Journal of Rheology* **1987**, 31, 683-697.

[36] Li, W.; Zhang, Y.; Yang J. Thermal Annealing Induced Enhancements of Electrical Conductivities and Mechanism for Multiwalled Carbon Nanotubes Filled Poly(Ethylene-co-Hexene) Composites. *Acs Appl Mater Interfaces* **2012**, 4, 6468-6478.

[37] Song, Y.; Zheng, Q. Linear viscoelasticity of polymer melts filled with nano-sized fillers. *Polymer* **2010**, 51, 3262-3268.

[38] Aghjeh, M.R.; Khonakdar, H.A.; Jafari, S.H. Application of mean-field theory in PP/EVA blends by focusing on dynamic mechanical properties in correlation with miscibility analysis. *Composites Part B Engineering* **2015**, 79, 74-82.

[39] Zhang, D.; He, M.; Qin, S.; Yu, J. Effect of fiber length and dispersion on properties of long glass fiber reinforced thermoplastic composites based on poly(butylene terephthalate). *Rsc Advances* **2017**, 7, 15439-15454.

[40] Ma, L.; Meng, L.; Wu, G. Improving the interfacial properties of carbon fiber-reinforced epoxy composites by grafting of branched polyethyleneimine on carbon fiber surface in supercritical methanol. *Composites Science & Technology* **2015**, 114, 64-71.

[41] Jiang, D.; Xing, L.; Liu, L.; Yan, X.; Guo, J. Interfacially reinforced unsaturated polyester composites by chemically grafting different functional POSS onto carbon fibers. *Journal of Materials Chemistry A* **2014**, 2, 18293-18303.

[42] Jiang, D.; Liu, L.; Long, J. Reinforced unsaturated polyester composites by chemically grafting amino-POSS onto carbon fibers with active double spiral structural spiralphosphodicholor. *Composites Science & Technology* **2014**, 100, 158-165.